APL Materials

# Single-crystalline $Cu_2O$ thin films of optical quality as obtained by the oxidation of single-crystal Cu thin films at low temperature

Cite as: APL Mater. 7, 031115 (2019); https://doi.org/10.1063/1.5087114
Submitted: 28 December 2018 . Accepted: 04 March 2019 . Published Online: 27 March 2019

Taewoo Ha, Inhee Park, Kyung Ik Sim, Howon Lee, Jong-Sung Bae, Su Jae Kim, Jong Phil Kim, Teun-Teun Kim, Jae Hoon Kim, Joon Ik Jang, and Se-Young Jeong

View Online
Export Citation
CrossMark

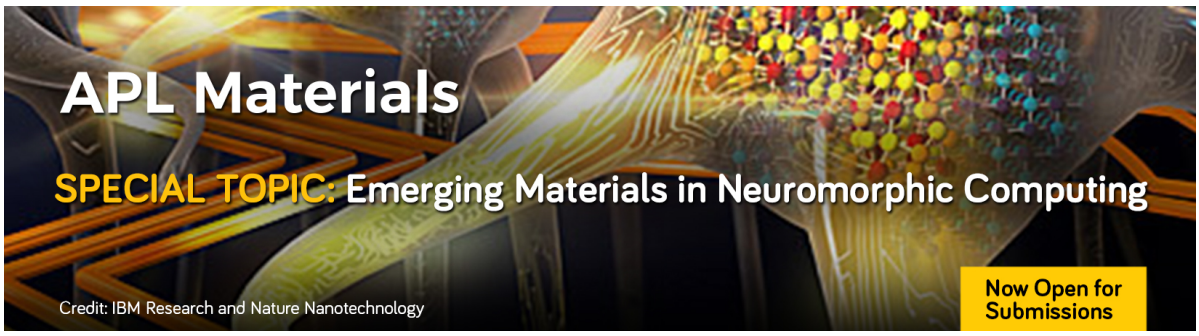




© 2019 Author(s).

# Single-crystalline $Cu_2O$ thin films of optical quality as obtained by the oxidation of single-crystal Cu thin films at low temperature

Cite as: APL Mater. 7, 031115 (2019); doi: 10.1063/1.5087114
Submitted: 28 December 2018 • Accepted: 4 March 2019 •
Published Online: 27 March 2019

View Online Export Citation CrossMark

Taewoo Ha,[1,2,3] Inhee Park,[4] Kyung Ik Sim,[1] Howon Lee,[1] Jong-Sung Bae,[5] Su Jae Kim,[6] Jong Phil Kim,[5] Teun-Teun Kim,[2,3] Jae Hoon Kim,[1,a)] Joon Ik Jang,[7,a)] and Se-Young Jeong[4,8,a)]

## AFFILIATIONS

[1]Department of Physics, Yonsei University, Seoul 03722, South Korea
[2]Center for Integrated Nanostructure Physics, Institute for Basic Science (IBS), Suwon 16419, South Korea
[3]Sungkyunkwan University (SKKU), Suwon 16419, South Korea
[4]Department of Cogno-Mechatronics Engineering, Pusan National University, Busan 46241, South Korea
[5]Division of Analysis and Research, Pusan Center, Korea Basic Science Institute, Busan 46742, South Korea
[6]Crystal Bank Research Institute, Pusan National University, Busan 46241, South Korea
[7]Department of Physics, Sogang University, Seoul 04107, South Korea
[8]Department of Optics and Mechatronics Engineering, Pusan National University, Busan 46241, South Korea

[a)]**Authors to whom correspondence should be addressed:** syjeong@pusan.ac.kr; jjcoupling@sogang.ac.kr; and super@yonsei.ac.kr

## ABSTRACT

High-quality, single-crystal-like $Cu_2O$ thin films of various thicknesses (10 nm–45 nm) were prepared at a low temperature (150 °C) by controlling layer-by-layer oxidation of wafer-scale Cu thin films sputtered along the (111) direction using a pure single-crystal Cu target. The cross-sectional images of the thin films reveal high crystallinity of $Cu_2O$ layers except for 60° twinning in the sequential stacking order as evidenced by high-resolution transmission electron microscopy, which is consistent with the absence of the photoluminescence (PL) signals arising from atomic-scale vacancies. The optical properties of our $Cu_2O$ films were investigated using temperature-dependent PL and Raman spectroscopy. All of the $Cu_2O$ thin films exhibit characteristic band-to-band transitions together with the series of yellow excitonic transitions slightly below the fundamental bandgap. The spectral locations for the PL are approximately consistent with those for the bulk counterpart. The excellent optical quality of our $Cu_2O$ was further demonstrated by significantly reduced quasi-direct transition that occurs at symmetry-breaking crystal imperfection, which relaxes the stringent momentum conservation rule. We identified the three main Raman scattering modes of the $Cu_2O$ thin films, where the two forbidden modes of $\Gamma_{15}^{(1)}$ and $\Gamma_{12}^{-} + \Gamma_{25}^{-}$ are resonantly allowed by the proximity of the incident photon energy to the green bandgap. We believe that our synthesis technique can be utilized for the preparation of single-crystal-like metal oxide thin films at low production temperatures with precise thickness control for the development of novel optoelectronic devices and for the exploration of the nanoscale light-matter interaction as well.

*© 2019 Author(s). All article content, except where otherwise noted, is licensed under a Creative Commons Attribution (CC BY) license (http://creativecommons.org/licenses/by/4.0/).* https://doi.org/10.1063/1.5087114

Metal oxides are one of the most abundant materials as they are typically more stable than their metallic counterparts. These materials are especially attractive when prepared into single-crystalline thin films with a sizable bandgap from the perspective of various applications involving photovoltaic, catalytic, optical, electric, and magnetic effects.[1–4] Therefore, it is of utmost importance to study


© Author(s) 2019

fundamental oxidation mechanisms and to establish the reproducible synthesis route for the mass production of high-quality oxide thin films on wafer scale. Among others, cuprous oxide ($Cu_2O$) is a non-toxic classical semiconductor that has been synthesized by various methods such as thermal oxidation, chemical oxidation, electro-deposition, reactive sputtering, activated reactive evaporation, rapid liquid dehydration and precipitation, filtered cathodic vacuum arc deposition, etc.[5–8] Unfortunately, however, most of these approaches rendered $Cu_2O$ thin films with significant amounts of defects and grains, thereby limiting their basic characterizations within structural and transport levels, especially because the subtle optical properties of this unique semiconductor are not likely retained in low-quality specimens.

Historically, $Cu_2O$ has been famous for the "forbidden-gap nature" that couples to its unusual crystal structure. As a consequence, both the lowest conduction band ($\Gamma_6^+$) built from Cu 4*s* levels and the highest valence band ($\Gamma_7^+$) from Cu 3*d* levels have positive parity at the zone center, causing a yellow ($\Gamma_6^+ \otimes \Gamma_7^+$) series with dipole-forbidden bandgap of 2.173 eV. More specifically, the yellow series has been at the core of fundamental exciton physics for studying long-lived excitonic matter and their relaxation dynamics with a special emphasis on excitonic Bose-Einstein condensation (BEC).[9–11] However, BEC in three-dimensional (3D) bulk $Cu_2O$ has been elusive,[12,13] even in the natural-growth crystal of extremely high optical quality.[14] Considering that excitonic BEC has been typically observed from two-dimensional microcavity systems,[15] the key to the success may lie in the synthesis of high-quality $Cu_2O$ thin films.[16–20] On the other hand, in view of device applications, high-quality $Cu_2O$ thin films must be assured for instance to be used as an active hole transport layer in $Cu_2O$-based solar cells, whose theoretical limit can reach as high as 20%. However, to the best of our knowledge, ultra-thin $Cu_2O$ films of such quality close to a single-crystal level have not been realized to this date.[21,22]

The structural and optical properties of deposited $Cu_2O$ films strongly depend on the fabrication method together with the selection of proper substrates.[23] For example, MgO substrates are typically used for fabricating epitaxial $Cu_2O$ thin films.[24–26] Using radio-frequency (RF) magnetron sputtering, epitaxial $Cu_2O$ thin films were synthesized on epitaxial ZnO (0001) substrates produced by molecular beam epitaxy (MBE).[27] However, critical issues still remain unresolved such as the oxygen partial pressure, high growth temperatures, and serious lattice mismatch. Alternatively, one can simply employ thermal oxidation for forming $Cu_2O$ films by heating copper sheets, which does not require any substrate. Obviously, in this case, the quality of the as-obtained $Cu_2O$ film is essentially determined by that of the starting Cu film. However, the lattice parameter of $Cu_2O$ is 1.65 times larger than that of Cu, and therefore, lattice distortion or grain formation during the oxidation process seems inevitable.[28,29] Nevertheless, minimized effects of strain must be assured for the fabrication of the oxide thin films having near perfect crystallinity.

Here, we report on the low-temperature synthesis of wafer-scale $Cu_2O$ thin films with thickness control in the range from 10 nm to 45 nm using phase-pure single-crystal Cu thin films obtained by a modified RF sputtering system.[30] The high quality of our $Cu_2O$ thin films was directly confirmed by employing the series of microscopic and spectroscopic characterization tools. The basic strategy of our approach is to start with highly phase-pure Cu films aligned perfectly along the (111) direction[30,31] and to control oxidation of the Cu layer in a thermal chamber at a low temperature of 150 °C under near ambient pressure. The atomic-scale images show high crystallinity of our $Cu_2O$ thin films.[30] Most intriguingly, the photoluminescence (PL) spectroscopy under UV illumination indicates highly suppressed quasi-direct transition at 3.211 eV, which typically appears from polycrystalline films and low-quality bulk crystals.[31] This observation implies the optical quality of our samples, which could be on par with natural-growth crystals especially in terms of the absence of the PL response arising from atomic-scale Cu and/or O vacancies. We believe that our technique can be readily generalized to obtain high-quality oxide films of wafer scale as long as phase-pure starting metal films are available by sputtering a single-crystal metal target. The processes below are optimum conditions about low temperature fabrication of ultra-thin $Cu_2O$ thin film.

**Fabrication of single-crystal Cu (111) thin films**. A 2-inch-diameter single-crystal Cu target was prepared from the Czochralski-grown Cu single-crystal ingot. Single-crystal Cu thin films were deposited on sapphire substrates (0001) using a radio-frequency sputtering system. During the sputtering process, the initial pressure was kept at ~$1.7 \times 10^{-5}$ torr. The working pressure was ~$5.3 \times 10^{-3}$ torr under Ar environment and the applied RF power was approximately 40 W.

**Thermal oxidation (Cu → $Cu_2O$)**. The thickness of the starting copper film works as a control parameter to determine the thickness (*d*) of the resulting $Cu_2O$ film. The oxidation of the Cu thin films was achieved by thermal treatment in a thermal furnace. The pressure of the furnace was about 1 atm while temperature was maintained at 150 °C. The typical size of the film specimens was about 10 mm × 10 mm obtained by cutting the 2-in Cu films prepared by RF sputtering.

We performed optical spectroscopic analysis of ultra-thin high quality $Cu_2O$ thin film through various optical measurement such as X-ray diffraction (XRD), X-ray photoelectron spectroscopy (XPS), scanning electron microscopy (SEM), atomic force microscopy (AFM), high-resolution transmission electron microscopy (HR-TEM), low-temperature PL, and Raman spectroscopy. Details of measurement conditions of all optical measurement are shown in the supplementary material.

Figure 1(a) shows the $\theta - 2\theta$ XRD spectra of $Cu_2O$ films with $d$ = 15 nm (black), 25 nm (red), and 35 nm (blue), respectively. The peak at $2\theta = 41.661°$ arises from the $Al_2O_3$ (001) substrate used for the fabrication of the Cu film, and the peak at 36.442° is assigned to $Cu_2O$ (111). The inset of Fig. 1(a) shows the strain-induced peak shift associated with the three different $d$ values of the $Cu_2O$ films in the $2\theta$ range from 35° to 38°. The shift of the peak position suggests that the strain effect varies depending on the thickness of the $Cu_2O$ film. While the peak position of the film with $d$ = 35 nm was observed at the same position as the reference of bulk $Cu_2O$ (Fig. S1), those of the 15- and 25-nm-thick film appear at slightly higher $2\theta$ values. This implies that the built-in stress induced from the substrate is relaxed with increasing thickness and disappears at around 35 nm. Figure 1(b) shows the φ scan of the $Cu_2O$ film ($d$ = 25 nm) exhibiting six-fold symmetry, which indicates that the $Cu_2O$ film is epitaxially well grown with high crystallinity and there are no other orientations. The φ scan of $Cu_2O$ oriented along the


© Author(s) 2019

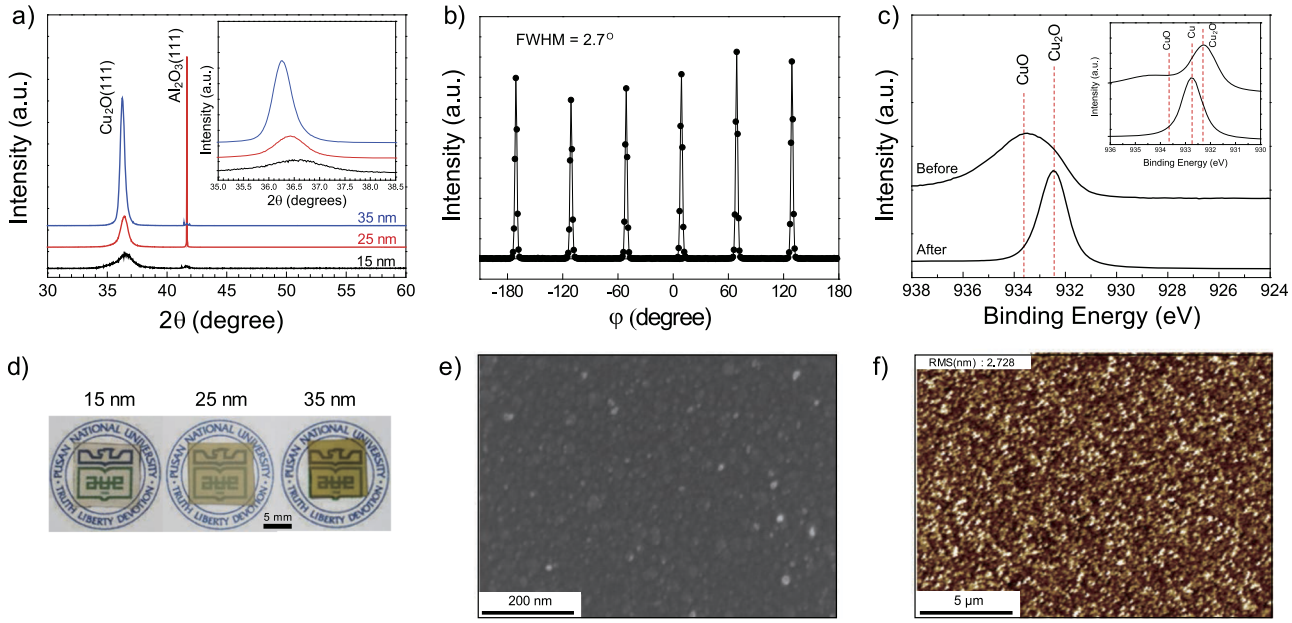


**FIG. 1**. (a) $\theta - 2\theta$ scan of $Cu_2O$ films with three different thicknesses ($d$ = 15 nm, 25 nm, and 35 nm) obtained using a synchrotron radiation source ($\lambda$ = 0.15 nm). The inset is the blow-up to show the peak shift upon thickness change. (b) φ scan and (c) XPS spectra of the $Cu_2O$ film ($d$ = 25 nm) before and after etching. The inset in (c) represents XPS spectra of a Cu thin film before and after etching. (d) Representative photos of our $Cu_2O$ films showing different levels of transparency for the three thicknesses. (e) SEM image and (f) AFM image of the $Cu_2O$ film ($d$ = 25 nm).

(111) direction actually should exhibit three-fold symmetry because it has a cubic structure. However, six-fold symmetry is caused by epitaxial twins having three-fold symmetry, but rotated by 60° each, as the Cu film used in this study has epitaxial twins rotated exactly by 60° in the epitaxial plane.[29] Similar φ scans were obtained from other samples.

Figure 1(c) shows the XPS results obtained from the $Cu_2O$ film before and after etching, clearly indicating that the surface of the $Cu_2O$ film (lower curve) is covered by CuO (upper curve). This implies that the Cu film completely turned to $Cu_2O$ after thermal treatment, but the surface of $Cu_2O$ is covered by a native CuO layer within ~2 or 3 nm, as CuO is more stable at the ambient.[33] For comparison, the inset shows those of a Cu thin film. It is evident that the as-prepared Cu film at the ambient has oxide layers, which can be completely removed with etching. Figure 1(d) shows the visual colors of our $Cu_2O$ films. The high-quality $Cu_2O$ films appear transparent yellow (not red as for the bulk counterpart) and become darker yellow as the thickness increases. We confirmed that low-quality $Cu_2O$ films exhibit opaque reddish color, which were obtained by oxidizing low-quality starting materials (Cu films). The yellow transparent color therefore only appears from high-quality $Cu_2O$ films. Figures 1(e) and 1(f) show representative SEM and AFM images of the $Cu_2O$ film, respectively. Both SEM and AFM images indicate that the $Cu_2O$ film have a smooth and uniform surface with a root-mean-square (RMS) roughness of 2.728 nm.

Figure 2(a) shows the cross-sectional TEM image of our $Cu_2O$ film. Although the original Cu film seemed to be transformed to $Cu_2O$ completely, the film is indeed composed of CuO, $CuO_x$, and $Cu_2O$ layers. The CuO layer is ~4 nm, which was 2 nm–3 nm as a natural oxide layer on the surface of the Cu thin film before oxidation. Just below the CuO layer, the $CuO_x$ layer was formed as an

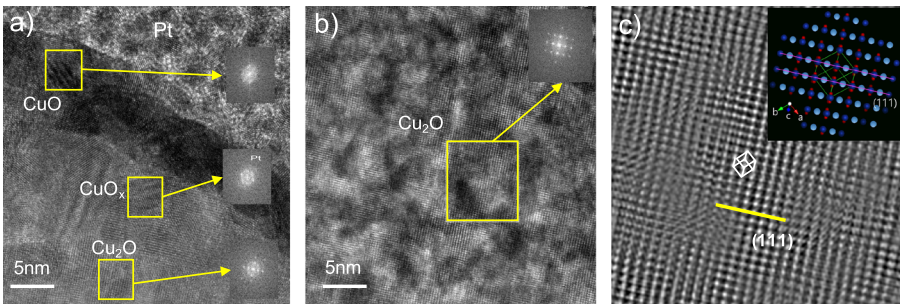


**FIG. 2**. (a) TEM image showing the formation of three layers of CuO, $CuO_x$, and $Cu_2O$ upon oxidation. (b) Pure $Cu_2O$ region. The inset in (b) shows FFT pattern of the yellow square. (c) Processed image from the FFT pattern of (b). The inset in (c) shows projection of a three-dimensional image using a crystallographic model. The yellow line indicates the projection of the (111) plane of $Cu_2O$.


© Author(s) 2019

interface layer between CuO and $Cu_2O$ with a thickness of ~4 nm. The three insets in Fig. 2(a) correspond to the fast Fourier transform (FFT) patterns of each selected square area. Compared with two other regions, the FFT pattern of the $Cu_2O$ phase shows much better crystallinity. To confirm the well-aligned $Cu_2O$ crystalline phase, an additional TEM image was taken at the center of the $Cu_2O$ layer as shown in Fig. 2(b), where the black/white contrast in the image was caused by focused ion beam milling for TEM. The FFT pattern of the selected square region is shown in the inset. The TEM image and its FFT pattern show excellent crystallinity of $Cu_2O$. Figure 2(c) is the processed image from the FFT pattern of Fig. 2(b).

For the better visualization of the crystal structure, a projection of a three-dimensional (3D) image was added in the inset, where the plane by spheres of sky blue for Cu atoms are shifted down by 1/2 from the plane by the spheres of deep blue for Cu atoms. The red spheres stand for oxygen atoms. The white box is a projection of the unit cell for the comparison of that in the inset, and the yellow line indicates the projection of the (111) plane. The TEM images unambiguously show that the $Cu_2O$ layer was well grown along the [111] direction.

Figure 3(a) schematically illustrates the band structure of $Cu_2O$ near the zone center with possible optical transitions indicated. The

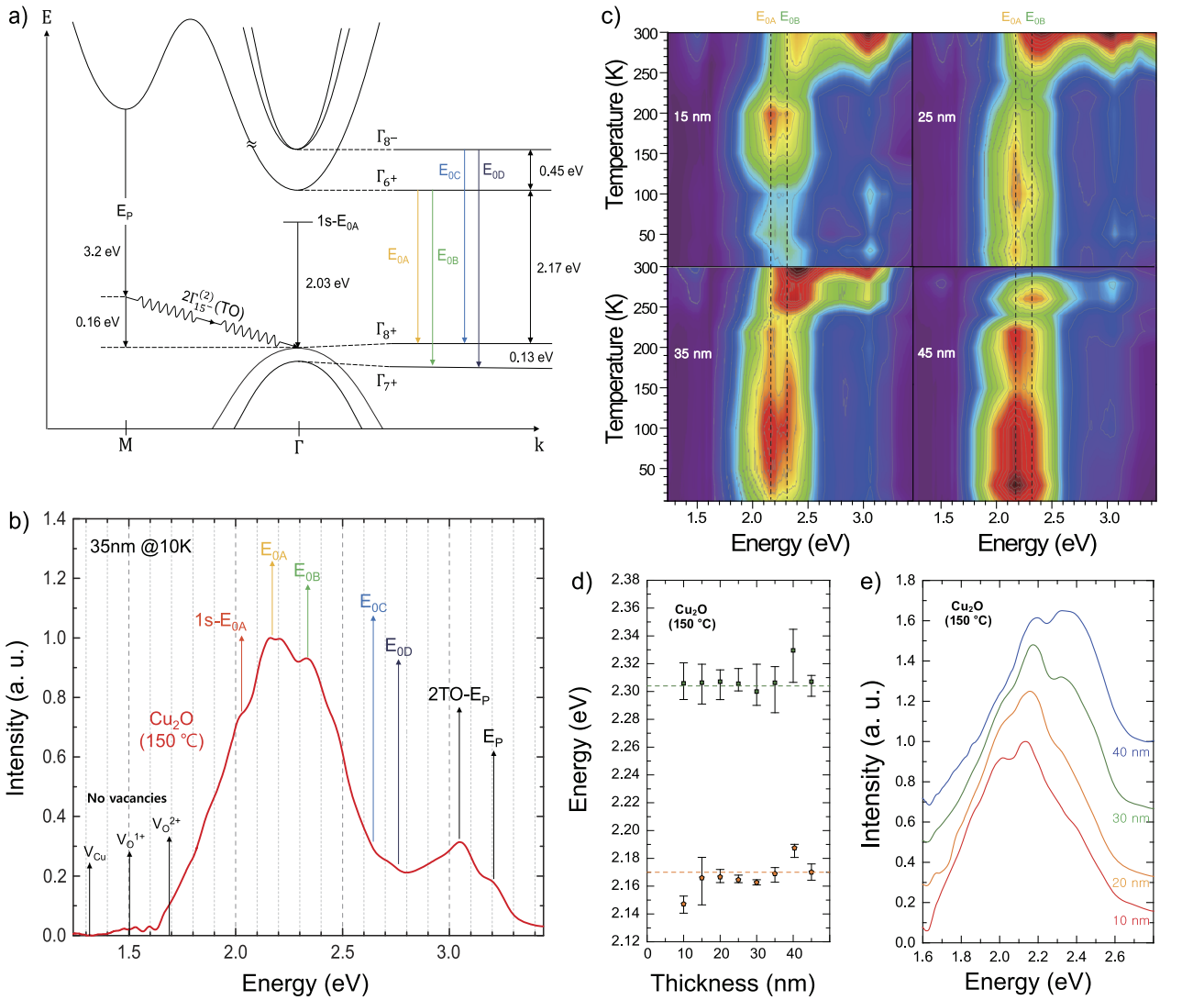


**FIG. 3**. (a) Schematic band structure of $Cu_2O$ across Γ and M points with major optical transitions specified. (b) PL spectra at 10 K from $Cu_2O$ thin films ($d$ = 35 nm). The spectral location for each optical transition is indicated. (c) Temperature-PL mapping of $Cu_2O$ thin films in the range from 10 to 300 K with specific film thickness of 15, 25, 35, and 45 nm, respectively. The spectral locations of $E_{0A}$ and $E_{0B}$ for the bulk case are marked by the dashed lines at 2.173 eV and 2.304 eV, respectively. (d) Thickness-dependence of $E_{0A}$ (orange dots) and $E_{0B}$ (green dots) of $Cu_2O$, determined by averaging the values below 100 K. (e) PL spectra at 10 K in the vicinity of yellow and green transitions observed from $Cu_2O$ thin films with $d$ = 10, 20, 30, and 40 nm.


© Author(s) 2019

transition across the fundamental bandgap is the yellow transition ($E_{0A}$) that involves the highest valence band ($\Gamma_8^+$) and the lowest conduction band ($\Gamma_6^+$), being separated by ~2.173 eV at 4 K.[34] The green transition ($E_{0B}$) occurs between the $\Gamma_6^+$ band and the second highest valence band ($\Gamma_7^+$), which is split from the ${}^+\Gamma_8$ band by spin-orbit coupling.[35] Direct transition across the yellow or the green gap is dipole forbidden as it occurs between the bands with same parity. In contrast, the blue ($E_{0C}$) and the indigo ($E_{0D}$) transitions are dipole allowed as they involve the second lowest conduction band ($\Gamma_8^-$) having opposite parity. Although the dipole-allowed transitions are more efficient, the yellow and the green transitions indeed dictate the PL response through indirect phonon-assisted transitions. All of the four transitions ($E_{0A}$, $E_{0B}$, $E_{0C}$, and $E_{0D}$) were observed from our samples in the PL measurements as indicated in Fig. 3(b). On the other hand, the additional features above 3.0 eV arise from the quasi-direct transition and its two-phonon side band ($E_P$ and 2TO-$E_P$). Considering that direct no-phonon transition is essentially a vertical process, it is rather surprising that $E_P$ is observed as this involves the conduction band at the M point and the valence band at the Γ point. However, this transition was even observed in a natural-growth sample,[32] which was attributed to imperfection of the crystal or grain boundaries where symmetry-breaking effects relax momentum conservation for the process. Therefore, this transition can be used as an "internal indicator" for the crystal quality of $Cu_2O$. In our high-quality thin films, the most probable source for grain boundaries is 60° symmetric rotation of a grain to neighboring grains. In fact, we emphasize that our $Cu_2O$ films are much higher quality compared with other polycrystalline films routinely obtained by oxidizing poor starting materials that actually show much stronger $E_P$ (3.211 eV); see, for example, Fig. 4 of Ref. 32.

The energy splitting between $E_P$ and 2TO-$E_P$ is approximately 0.158 eV and close to twice the energy for the infrared-allowed transverse optical (TO) phonon with the value of 78.5 meV (Fig. S5).[36] The absence of the one-phonon peak is due to the centrosymmetric nature of $Cu_2O$, where single-phonon emission flips the parity. There are two possible origins for this two-phonon transition (3.053 eV). It may simply correspond to the two-phonon overtone with the two phonons having opposite momenta, causing the transition within the M point. If this is the case, 2TO-$E_P$ should be weaker than $E_P$ because the indirect photon transition is a higher order process compared with the direct no-phonon transition: This trend was indeed observed from typical $Cu_2O$ thin films of nominal quality.[32] Alternatively, the two-phonon transition can occur between the zone boundary and the center (M-Γ) as momentum mismatch can be carried by successive emission of two TO phonons with the same momenta toward the Γ point, which is a horizontal process. Since the phonon line (2TO-$E_P$) is noticeably stronger than the direct line ($E_P$) in our $Cu_2O$ thin films, the latter process seems to be more important in our case, which in turn implies high crystallinity of our thin films, as the horizontal process does not need any extrinsic symmetry breaking (Fig. S2).

Generally, optical transitions at the vacancy sites are more frequent at low temperatures since Coulomb attraction of carriers and/or excitons by ambient atomic-scale defects is stronger at lower temperatures. Even in natural-growth $Cu_2O$ single crystals, such transitions are typically observed at 1.3, 1.5, and 1.7 eV, which arise from radiative recombination at copper vacancies ($V_{Cu}$), singly charged oxygen vacancies ($V_O^{1+}$), and doubly charged oxygen vacancies ($V_O^{2+}$), respectively.[32,37,38] However, our $Cu_2O$ thin films showed no clear vacancy peaks at a sufficiently low temperature of 10 K (Fig. S2). We could also find the clear interband transition of our $Cu_2O$ thin film even at the thinnest film of 10 nm as shown in Fig. S4.

Figure 3(c) shows 2D mappings of the PL spectra of $Cu_2O$ (150 °C) vs. temperature (10 K–300 K) for four different thicknesses ($d$ = 15, 25, 35, and 45 nm). Both $E_{0A}$ and $E_{0B}$ transitions are reasonably well identified for all of our samples, where the two dashed lines correspond to the bulk values of 2.173 eV and 2.304 eV, respectively. For the case of thinner films ($d \leq 15$ nm), however, the characteristic PL features diminish below 100 K presumably because of instability of the $Cu_2O$ phase induced by partial transformation into the intermediate $CuO_x$ phase. This effect is supposed to be less important for thicker samples. In general, the 2TO-$E_P$ transition (3.053 eV) plummets with decreasing temperature as the thermal population of high-energy TO phonons steeply drops at lower temperatures. Interestingly, however, it was found that this transition can revive even at very low temperatures whenever the main band-edge transitions become weaker; see, for example, $d$ = 15 nm (10 K < $T$ < 100 K), $d$ = 25 nm (10 K < $T$ < 50 K), or $d$ = 35 nm ($T$ ~ 10 K). This anomaly may arise from unusual lattice expansion and phase transition behaviors of $Cu_2O$,[29,36] which needs more investigations for understanding the exact mechanism. Both $E_{0A}$ and $E_{0B}$ transitions become more articulate with increasing thickness. We believe that the thickest film ($d$ = 45 nm) is especially in high quality based on intense yellow transitions at low temperatures with almost no PL response relevant to quasi-direct transition and its two-phonon line (Fig. S3).

Figure 3(d) shows the spectral locations for $E_{0A}$ and $E_{0B}$, determined from our films. Significant overlap of the yellow and the green PL bands causes a rather large uncertainty in the precise locations for the transitions. The spectroscopically determined energy separation between $E_{0A}$ and $E_{0B}$ of our thin films corresponds to spin-orbit splitting energy between the two valence bands of $\Gamma_7^+$ and $\Gamma_8^+$, which is around 0.14 ± 0.01 eV. This value is similar to the value of 0.131 eV in the bulk. The spectral locations for the two peaks seem to persist within the experimental error-bar range independent of the thickness for the films. Figure 3(e) shows the PL spectra in the vicinity of the yellow and green transitions observed from the $Cu_2O$ thin films ($d$ = 10, 20, 30, and 40 nm). Despite the above-mentioned PL band overlap, the PL features below the yellow gap clearly indicate the case for excitonic emission (1s-$E_{0A}$), consisting of not only direct transition but also several phonon replicas. As the thickness of the film increases, the green transitions gradually become dominant, rendering the yellow PL peaks relatively less pronounced.

Figure 4(a) shows Raman spectra of our $Cu_2O$ thin films obtained by using 532 nm excitation that were fit by the three Lorentzian peaks. The observed Raman signals are identified as follows: The orange spectral area indicates the infrared active phonon mode of $Cu_2O$ $\Gamma_{15}^{(1)}$ (149 $cm^{-1}$); the green spectral area is the two-phonon combination mode of $\Gamma_{12}^-$ and $\Gamma_{25}^-$ (198 $cm^{-1}$); the blue spectral area is the second-order overtone of the main Raman signal of $2\Gamma_{12}^-$ (218 $cm^{-1}$). In principle, only the latter mode should be active according to the parity selection rules.[36,39,40] The $2\Gamma_{12}^-$


© Author(s) 2019

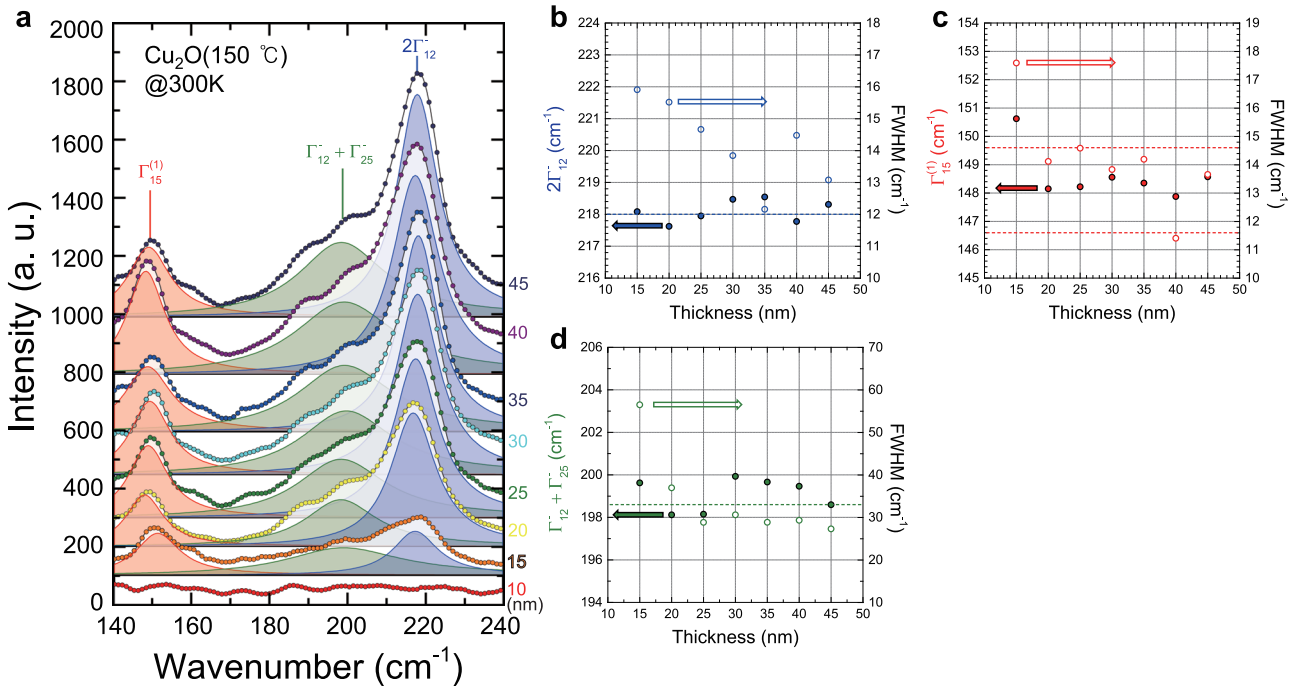


**FIG. 4**. (a) Series of the Raman spectra of $Cu_2O$ thin films with the controlled thickness in the range from 10 nm to 45 nm as represented by the coloured symbols. Each spectrum was fitted to identify the associated phonon modes of $\Gamma_{15}^{(1)}$ (149 $cm^{-1}$), $\Gamma_{12}^- + \Gamma_{25}^-$ (198.6 $cm^{-1}$), and $2\Gamma_{12}^-$ (218 $cm^{-1}$), as marked by the red, green, and blue color-filled traces with Lorentzian shape, respectively. Thickness-dependent mode frequencies and FWHM of (b) $\Gamma_{15}^{(1)}$, (c) $\Gamma_{12}^- + \Gamma_{25}^-$, and (d) $2\Gamma_{12}^-$, respectively. The dashed line in each plot indicates the experimental values for the transverse and longitudinal optical phonon modes adopted from Ref. 40.

mode does not show any significant changes with thickness, and its value is close to the reported one in a single-crystal, as indicated by the blue dashed line in Fig. 4(b). We did not observe any clear Raman signal from the thinnest $Cu_2O$ ($d$ = 10 nm) as the active thickness of the $Cu_2O$ layer is just ~3 nm–4 nm according to the TEM data in Fig. 2(a). Figure 4(b) also shows the full width at the half maximum (FWHM) of the $2\Gamma_{12}^-$ mode (open circle) as a function of $d$, indicating improved crystallinity for thicker films up to 45 nm. A similar trend was observed from the other modes. In fact, the infrared active $\Gamma_{15}^{(1)}$ has two closely located TO (18.8 meV) and one LO (19.1 meV) modes as indicated by the two dashed lines in Fig. 4(c).[41] Although this peak is not predicted to occur according to the selection rules, it seems to arise from the Raman resonance effect as the excitation line is close enough to the green bandgap.[42] Therefore, it is not surprising to also observe the forbidden $\Gamma_{12}^- + \Gamma_{25}^-$ mode throughout our samples because of the same reason. In fact, similar effects were typically observed from high-quality natural-growth crystals when the incident photon energy is resonant with the yellow exciton series.[43–46] The experimental Raman frequencies in Figs. 4(b)–4(d) were obtained by three Lorentzian fitting in Fig. 4(a) and show a good agreement with the previous results (dashed lines).

We have synthesized high-quality thin films of single-crystalline $Cu_2O$ with thickness control (10 nm–45 nm) by layer-by-layer oxidation of highly phase-pure Cu films sputtered on the sapphire substrates at a relatively low temperature (150 °C) under near ambient pressure. The structural properties of these films were directly assessed by XRD, XPS, SEM, AFM and high-resolution TEM, which all revealed high crystallinity of $Cu_2O$ oriented along the (111) direction with in-plane grains most likely arising from 60° epitaxial twins. We examined the thickness-dependent optical properties of our thin films based on both PL and Raman spectroscopy, which indicate gradual evolution of the characteristic peaks towards those of the bulk counterpart with increasing thickness. We emphasize that previous investigations of the epitaxial $Cu_2O$ thin films were rather restricted to structural and transport measurements because of relatively poor film qualities for precision optical characterization. In a sharp contrast, all of our films exhibited four major band-to-band transitions together with excitonic response, which manifest themselves more intensely as the temperature was reduced. Considering that even high-quality natural-growth $Cu_2O$ crystals typically exhibit strong optical transition arising from atomic-scale Cu and/or O vacancies, the absence of these defect transitions clearly indicates the exceptional quality of our epitaxial $Cu_2O$ thin films. This was also further demonstrated by highly suppressed quasi-direct transition $E_P$, when compared with other synthetic $Cu_2O$ films, which is an internal indicator for the crystal quality. Typical Raman modes of a bulk $Cu_2O$ were also observed from our $Cu_2O$ thin films that undergo measureable shift upon thickness control. The appearance of the two forbidden modes can be attributed to a resonance effect, which is not relevant to any extrinsic symmetry-breaking effect of low crystallinity. We believe that our unique synthesis approach


© Author(s) 2019

can be further optimized for producing even better qualities of thin $Cu_2O$ films that can be used for studying various excitonic matter in the 2D landscape. This may include quadrupole polaritions and their condensation when prepared within the microcavity environment.

See supplementary material for details of the proposed XRD, temperature dependent PL, Raman spectroscopy, and analysis of the experimental results of $Cu_2O$ thin film. Additional information of measurement methods of XRD, XPS, SEM, AFM, HRTEM, PL, and Raman spectroscopy is included.

J.H.K. acknowledges support by the National Research Foundation of Korea (NRF) grants funded by the Ministry of Science, ICT, and Future Planning (MSIP) of Korea (NRL Program Nos. NRF-2015R1A2A2A01005288 and NRF-2015R1A2A1A03066171, SRC Program No. NRF-2017R1A5A1014862). S.-Y.J. acknowledges support by the Basic Science Research Program through the NRF of Korea funded by the Ministry of Science, ICT, and Future Planning (No. NRF-2017R1A2B3011822). J.I.J. acknowledges support by the Basic Research Program (No. NRF-2017R1D1A1B03035539) through the NRF of Korea funded by the Korean government. This work was also partially supported by IBS-R011-D1.

## REFERENCES

[1] X. Yu, T. J. Marks, and A. Facchetti, Nat. Mater. **15**, 383 (2016).
[2] L. Pan, J. H. Kim, M. T. Mayer, M.-K. Son, A. Ummadisingu, J. S. Lee, A. Hagfeldt, J. Luo, and M. Grätzel, Nat. Catal. **1**, 412 (2018).
[3] S. V. Kalinin and N. A. Spaldin, Science **341**, 858 (2013).
[4] S. Lany, J. Phys.: Condens. Matter **27**, 283203 (2015).
[5] A. E. Rakhshani, Solid State Electron **29**, 7 (1986).
[6] B. Balamurugan, B. R. Mehta, and S. M. Shivaprasad, Appl. Phys. Lett. **79**, 3176 (2001).
[7] V. R. Palkar, P. Ayyub, S. Chattopadhyay, and M. Multani, Phys. Rev. B **53**, 2167 (1996).
[8] Z. H. Gan, G. Q. Yu, B. K. Tay, C. M. Tan, Z. W. Zhao, and Y. Q. Fu, J. Phys. D: Appl. Phys. **37**, 81 (2004).
[9] J. I. Jang and J. P. Wolfe, Phys. Rev. B **74**, 045211 (2006).
[10] K. E. O'Hara and J. P. Wolfe, Phys. Rev. B **62**, 12909 (2000).
[11] J. P. Wolfe, J. L. Lin, and D. W. Snoke, "Bose-Einstein condensation of a nearly ideal gas: Excitons in $Cu_2O$," in *Bose-Einstein Condensation*, edited by A. Griffin, D. W. Snoke, and S. Stringari (Cambridge University Press, Cambridge, 1995), Chap. 13, p. 281.
[12] K. Yoshioka, E. Chae, and M. Kuwata-Gonokami, Nat. Commun. **2**, 328 (2011).
[13] R. Schwartz, N. Naka, F. Kieseling, and H. Stolz, New J. Phys. **14**, 023054 (2012).
[14] T. Kazimierczuk, D. Frohlich, S. Scheel, H. Stolz, and M. Bayer, Nature **514**, 343 (2014).
[15] H. Deng, H. Haug, and Y. Yamamoto, Rev. Mod. Phys. **82**, 1489 (2010).
[16] N. Naka, S. Hashimoto, and T. Ishihara, Jpn. J. Appl. Phys. **44**, 5096 (2005).
[17] K. Iwamitsu, S. Aihara, T. Shimamoto, A. Fujii, and I. Akai, Eur. Phys. J. B **86**, 194 (2013).
[18] M. Takahata, K. Tanaka, and N. Naka, Phys. Rev. B **97**, 205305 (2018).
[19] M. Takahata, K. Tanaka, and N. Naka, Phys. Rev. Lett. **121**, 173604 (2018).
[20] Z. G. Yin, H. T. Zhang, D. M. Goodner, M. J. Bedzyk, R. P. H. Chang, Y. Sun, and J. B. Ketterson, Appl. Phys. Lett. **86**, 061901 (2005).
[21] T. Narushima, H. Tsukamoto, and T. Yonezawa, AIP Adv. **2**, 042113 (2012).
[22] Y. Z. Hu, R. Sharangpani, and S. P. Tay, J. Electrochem. Soc. **148**, G669 (2001).
[23] Y. Sun, Ph.D. thesis, Northwestern University, Evanston, 2001.
[24] B. K. Meyer, A. Polity, D. Reppin, M. Becker, P. Hering, P. J. Klar, T. Sander, C. Reindl, J. Benz, M. Eickhoff, C. Heiliger, M. Heinemann, J. Bläsing, A. Krost, S. Shokovets, C. Müller, and C. Ronning, Phys. Status Solidi B **249**, 1487 (2012).
[25] Y. Sun, K. Rivkin, J. Chen, and J. B. Ketterson, Phys. Rev. B **66**, 245315 (2002).
[26] P. R. Markworth, R. P. H. Chang, Y. Sun, G. K. Wong, and J. B. Ketterson, J. Mater. Res. **16**, 914 (2001).
[27] J. Gan, S. Gorantla, H. N. Riise, Ø. S. Fjellvåg, S. Diplas, O. M. Løvvik, B. G. Svensson, E. V. Monakhov, and A. E. Gunnæs, Appl. Phys. Lett. **108**, 152110 (2016).
[28] B. Maack and N. Nilius, Thin Solid Films **651**, 24 (2017).
[29] S. Mani, J. I. Jang, J. B. Ketterson, and H. Y. Park, J. Cryst. Growth **311**, 3549 (2009).
[30] S. Lee, J. Y. Kim, T. W. Lee, W. K. Kim, B. S. Kim, J. H. Park, J. S. Bae, Y. C. Cho, J. Kim, M. W. Oh, C. S. Hwang, and S. Y. Jeong, Sci. Rep. **4**, 6230 (2014).
[31] V. L. Nguyen, D. J. Perello, S. Lee, C. T. Nai, B. G. Shin, J. G. Kim, H. Y. Park, H. Y. Jeong, J. Zhao, Q. A. Vu, S. H. Lee, K. P. Loh, S. Y. Jeong, and Y. H. Lee, Adv. Mater. **28**, 8177 (2016).
[32] J. W. Park, H. Jang, S. Kim, S. H. Choi, H. Lee, J. Kang, and S. H. Wei, J. Appl. Phys. **110**, 103503 (2011).
[33] A. Soon, M. Todorova, B. Delley, and C. Stampfl, Phys. Rev. B **76**, 129902 (2007).
[34] P. W. Baumeister, Phys. Rev. **121**, 359 (1961).
[35] T. Ito, T. Kawashima, H. Yamaguchi, T. Masumi, and S. Adachi, J. Phys. Soc. Jpn. **67**, 2125 (1998).
[36] M. Ivandam, D. Waasmaier, A. Endriss, J. Ihringer, A. Kirfel, and W. Kiefer, J. Raman Spectrosc. **28**, 487 (1997).
[37] T. Ito and T. Masumi, J. Phys. Soc. Jpn. **66**, 2185 (1997).
[38] M. Zouaghi, B. Prevot, C. Carabatos, and M. Sieskind, Phys. Status Solidi A **11**, 449 (1972).
[39] M. Balkanski, M. A. Nusimovici, and J. Reydellet, Solid State Commun. **7**, 815 (1969).
[40] W. Yu, M. Han, K. Jiang, Z. Duan, Y. Li, Z. Hu, and J. Chu, J. Raman Spectrosc. **44**, 142 (2013).
[41] P. Dawson, M. M. Hargreave, and G. R. Wilkinson, J. Phys. Chem. Solids **34**, 2201 (1973).
[42] P. Y. Yu and Y. R. Shen, Phys. Rev. B **17**, 4017 (1978).
[43] A. Compaan and H. Z. Cummins, Phys. Rev. Lett. **31**, 41 (1973).
[44] P. F. Williams and S. P. S. Porto, Phys. Rev. B **8**, 1782 (1973).
[45] A. Compaan, Solid State Commun. **16**, 293 (1975).
[46] P. Y. Yu and Y. R. Shen, Phys. Rev. B **12**, 1377 (1975).


© Author(s) 2019